Catalytic Ortho–Parahydrogen Conversion Over Platinum Group Metals (PGM)

Malak El Tfayli[1], Mojtaba Gohari Bahabadi[2,3], Liangguang Tang[3], Doki Yamaguchi[3], Thomas J. Hughes[2], and Arman Siahvashi[1*]

[1] School of Aeronautical, Mechanical and Mechatronic Engineering, The University of Sydney, Australia.
[2] Department of Civil and Environmental Engineering, Monash University, Australia.
[3] Commonwealth Scientific and Industrial Research Organization, Melbourne, Australia.

[*]E-mail: arman.siahvashi@sydney.edu.au

Abstract. Efficient ortho-parahydrogen conversion (OPC) is essential for minimising boil off losses during hydrogen liquefaction and storage. This study compares the OPC performance of iron oxide catalyst from Molecular Products (commercially known as IONEX) with supported Platinum Group Metals (PGM) catalysts, which include 5 wt% Ru, Rh, and Pt supported on Al_2O_3. Catalyst samples with a 1 g mass were evaluated at 77 K and 1.2 barg over hydrogen flow rates of 0.3–3.0 SLPM. Outlet parahydrogen fractions were measured using a thermal conductivity detector, and apparent rate constants were determined using a first order kinetic model. The Rh/Al_2O_3 and Ru/Al_2O_3 catalysts exhibited rate constants of 483 and 401 min^{-1}, respectively, compared with 214 min^{-1} for IONEX, while Pt/Al_2O_3 catalyst showed negligible activity at 13 min^{-1}. Structural, surface, and magnetic characterisation indicated that PGM activity is consistent with a dissociation recombination mechanism, distinct from the non-dissociative magnetic mechanism associated with IONEX. These findings identify Rh and Ru as promising catalysts for reducing converter size, pressure drop, energy losses, and costs in future industrial hydrogen liquefaction processes.

1. Introduction

Hydrogen is increasingly recognised as a key energy carrier for decarbonising transport, industry, and long duration energy storage. Liquid hydrogen (LH_2) is particularly attractive for applications requiring compact storage because its volumetric energy density is approximately 1.7 times that of hydrogen compressed up to 700 bar [1]. However, hydrogen liquefaction remains energy intensive, with 15-20% of the overall energy demand arising from the conversion between its nuclear spin isomers, orthohydrogen (oH_2) and parahydrogen (pH_2) [2].

At ambient temperature, equilibrium hydrogen consists of approximately 25% pH_2, whereas at 20 K, the normal boiling point of hydrogen, equilibrium composition approaches 100% pH_2 [3]. If this conversion is not completed during liquefaction, the exothermic ortho to para conversion (OPC) continues to storage. The released heat in this conversion (702 kJ/kg) far exceeds the latent heat of vaporization (448 kJ/kg) which causes LH_2 to evaporate, potentially boiling off 50% of LH_2 within 10 days [4, 5]. This conversion contributes approximately 0.59 kWh/kg LH_2, or 15% of the minimum reversible liquefaction work. In an optimised 5 TPD (metric tonnes per day) continuous conversion process, the exergy consumed in removing the conversion heat was approximately

0.67 kWh/kg LH_2, equivalent to about 5.9% of the total SEC (specific energy consumption) [2]. Management of this conversion is therefore essential for maintaining product quality, minimising hydrogen boil off and improving the economic performance of liquefaction and storage systems.

Industrial hydrogen liquefaction cycles address this requirement by incorporating catalytic OPC stages within their heat exchanger trains as hydrogen is progressively cooled to approximately 20 K [5]. The conventional catalyst is iron oxide from Molecular Products which is commercially available as IONEX to promote conversion through interactions between hydrogen molecules and inhomogeneous magnetic fields at the catalyst surface [6, 7]. Although effective, IONEX has limited activity, is sensitive to activation conditions and deactivation, and requires large catalyst volumes to achieve conversion. These limitations increase converter size, pressure drop, SEC, plant footprint, and capital cost [3, 8].

Platinum group metals (PGMs), including ruthenium, rhodium, and platinum, offer a potential alternative. These metals effectively activate molecular hydrogen through dissociative adsorption in hydrogenation, dehydrogenation, and fuel cell reactions [3, 8]. Nevertheless, their performance in OPC remains insufficiently investigated, particularly through direct comparison with IONEX under matched cryogenic conditions. This study experimentally compares IONEX with 5 wt% Ru, Rh, and Pt catalysts supported on Al_2O_3 at 77 K and 1.2 barg. Their conversion kinetics, structural characteristics, and magnetic properties are examined to clarify the underlying catalytic mechanisms.

2. Experimental

2.1 Catalysts and Activation Procedure

The overarching aim of this study is to compare the OPC activity of PGM catalysts against the industry standard IONEX catalyst. Four catalysts were tested: 30-50 mesh IONEX particles (from Molecular Products) and 5 wt% Ru, Rh, and Pt supported on Al_2O_3 particles of 70 μm average reported particle size (from BASF). All catalysts were tested using samples with a mass of 1 g at a reaction temperature of 77 K, a gauge pressure of 1.2 barg, and a hydrogen flow rate of 0.3 to 3 SLPM.

Prior to testing, each catalyst was activated to remove surface contaminants and generate active metal sites. PGM catalysts were activated with 2 hours of evacuation followed by 2 hours of hydrogen flow at T= 473 K. IONEX was activated under vacuum alone for 4 hours at T=453 K. Different activation mechanisms were used for each catalyst based on our previous internal tests and literature reports on ideal activations for each catalyst. Ruthenium was found to have best activation when reduced under high temperature with hydrogen exposure, whereas IONEX was found to lose activity at temperatures beyond 453 K [9-11].

2.2 Ortho-Parahydrogen Measurement

The ortho-parahydrogen measurements were conducted at CSIRO's Hydrogen Technology Development Facility using a cryogenic flow rig as shown in Figure 1. Grade 5 hydrogen (99.999%), further purified with hydrogen purifier from VICI [12], was supplied through the gas panel to the thermal conductivity detector (TCD). The TCD was calibrated against normal hydrogen (25% pH_2) exiting the normalizer and 100% pH_2 that was estimated from the properties of a 3.5% He in H_2 mixture, as recommended by the manufacturer [13].

At the start of each test, a mass of 1 g of catalyst was loaded into the reactor which is a 50 mm long ½" stainless steel tube that was supported with steel mesh and Quartz wool under the catalyst bed. For activation, the reactor was wrapped with a heating element and heated for 4 h

according to section 2.1. After activation the reactor was cooled to room temperature while the TCD was calibrated. The reactor and upstream cooling coil were then immersed in liquid nitrogen to reach a temperature of 77 K, with purified hydrogen flowing at a flow rate of 0.3 SLPM and a pressure of 1.2 barg. The outlet pH_2 fraction was measured at flow rates of 0.3, 0.5, 1.0, 1.5, 2.0, 2.5, and 3.0 SLPM. After testing, the reactor was removed from the dewar, and the catalyst was recovered for characterization according to section 2.4. These measurements were then used to calculate the rate constant, as described in section 2.3.

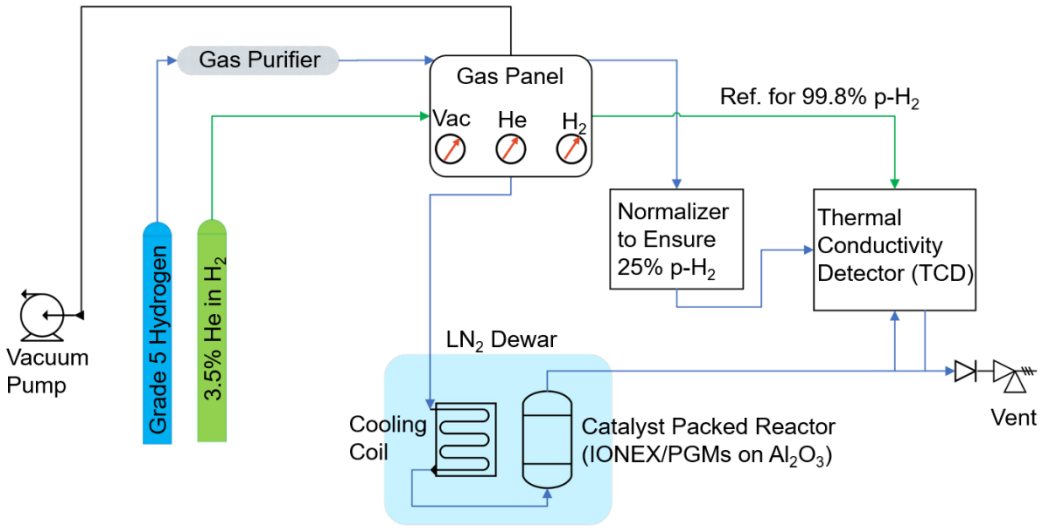

Figure 1: Process flow diagram of the experimental setup at the Hydrogen Technology Development Facility in CSIRO.

2.3 Rate constant evaluation

The rate constant k was calculated using the first order rate law:

$$x_2 = x_{eq} - (x_{eq} - x_1)e^{-\frac{k}{SV}} \quad (1)$$

Where SV is the space velocity (the volumetric flow rate at the actual reaction temperature and pressure divided by the volume of catalyst), x_{eq} is pH_2 equilibrium fraction at 77 K (50.2%), x_1 is the reactor inlet fraction (24.9%), and x_2 is the measured outlet fraction. The rate constant was obtained by solving for the least residual sum of squares between experimental and model predicted outlet fraction as shown in equation 2:

$$RSS = \sum_{i=1}^{N} (x_{exp} - x_{pred})^2 \quad (2)$$

The propagated uncertainty in the calculated rate constant (Δk) was calculated from the average values of Δk across the measured flowrates and pH_2 fractions as:

$$\Delta k = \frac{SV}{x_{eq} - x_2} \Delta x_2 \quad (3)$$

where Δx_2 is the uncertainty in outlet pH_2 fraction measured by the TCD given by the manufacturer as 1% pH_2 [13]. It should be noted that uncertainties in the measured flow rates and pressures also contribute to the calculated space velocity (SV). However, their contribution

to the propagated uncertainty in the calculated rate constant is negligible compared with the 1% uncertainty in the measured pH_2 fraction [11].

2.4 Material characterization

Fresh and post-reaction catalysts were characterized to relate measured activity to underlying structure and mechanism. The pore diameter, specific surface area, and particle size were quantified from BET adsorption isotherms where samples were degassed at 393 K then adsorption and desorption measurements were made with nitrogen at 77 K. The magnetic behaviour and susceptibility were measured via vibrating sample magnetometry where the sample magnetic moment was measured for 5 mg of each sample under the effect of varying the magnetic field between -40 T and 40 T at 77 K.

3. Results and Discussion

The activities of the four catalysts were evaluated at 77 K by measuring the pH_2 fraction at the reactor outlet over a range of space velocities, as displayed in Figure 2(A). For all catalysts, the outlet pH_2 fraction decreased with increasing space velocity because of the corresponding reduction in residence time. However, 5 wt% Rh/Al_2O_3 maintained the highest conversion across the investigated range. As shown in the rate constant values in Figure 2(B), the rate constants of Rh/Al_2O_3 and Ru/Al_2O_3 were 483 and 401 min^{-1}, respectively, corresponding to 2.26 and 1.87 times the value obtained for IONEX (214 min^{-1}). In contrast, Pt/Al_2O_3 exhibited a rate constant of only 13 min^{-1}, equivalent to 6.1% of the IONEX value.

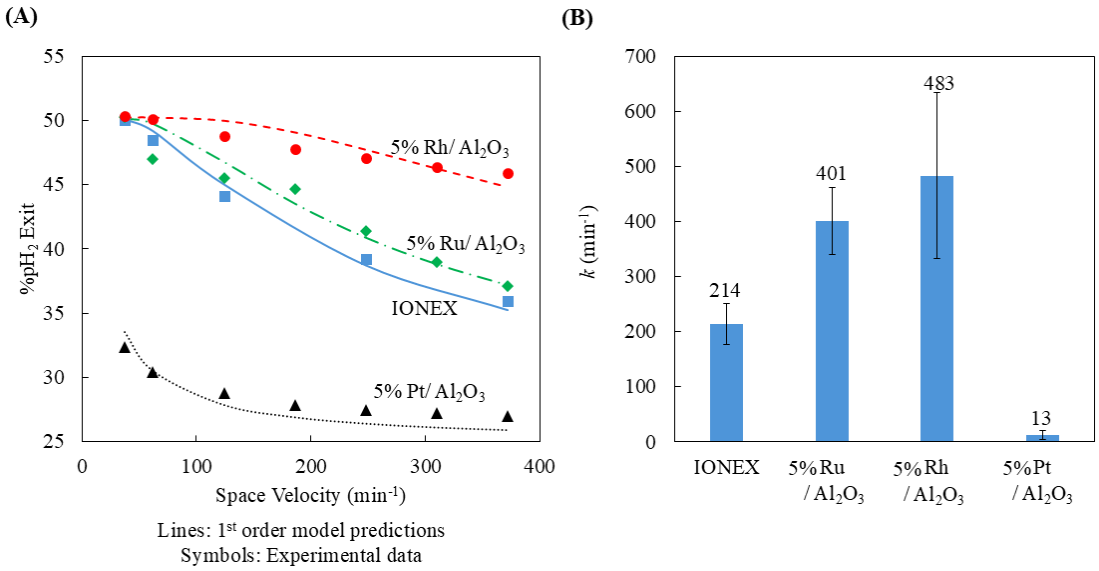

Figure 2: OPC activity of the tested catalysts at 77 K and 1.2 barg. (A) Experimental outlet pH_2 fraction and 1st order model predictions vs space velocity. (B) Apparent 1st order rate constants fitted from experimental data with propagated uncertainty.

These observations motivated further material characterisation to investigate the mechanisms governing catalyst performance. IONEX exhibited approximately twice the specific surface area of the PGM catalysts (184.8 versus an average of 91.3 $m^2.g^{-1}$), a higher nominal fraction of the active phase, and the highest magnetic susceptibility (χ=3.2x10^{-3} emu/g.Oe), as summarised in Tables 1 and 2. Nevertheless, the 5 wt% Rh/Al_2O_3 material, which exhibited diamagnetic behaviour and has almost half specific surface area, achieved the highest conversion

rate. These results suggest that the magnetic mechanism responsible for non-dissociative conversion over IONEX may not govern conversion over the PGM catalysts [14]. Instead, the observed activity is consistent with a mechanism involving H_2 dissociation, adsorption, recombination, and desorption on the metal surface [14]. In this mechanism, catalyst performance is influenced by the metal's ability to bind and subsequently release hydrogen. The hydrogen binding energies reported in the literature (Table 2) provide further support for this proposed mechanism. Ruthenium and rhodium exhibit highest binding energies, favouring the dissociative mechanism, whereas platinum exhibits around half the binding energy and the lowest magnetic susceptibility making it the least active catalyst under both mechanisms.

Table 1. Catalyst physical characteristics obtained via adsorption isotherm analysis.

Catalyst	Average pore diameter (nm)	Specific surface area (m^2/g)	Average particle size (μm)
IONEX	4.5	184.8	362
5% Ru/ Al_2O_3*	10.6	91.3	77

* Physical characteristics of PGM catalysts are similar since they're controlled by the common underlying support (Al_2O_3 particles). Therefore, the values from one sample were reported.

Table 2. Magnetic susceptibility and hydrogen binding energy of the given catalysts.

Catalyst	Magnetic susceptibility χ (emu/g.Oe)	Binding energy Eb (kJ/mol)
IONEX	3.2×10^{-3}	Null
5% Rh/Al_2O_3	Diamagnetic	78*
5% Ru/Al_2O_3	1.6×10^{-5}	70*
5% Pt/Al_2O_3	1.5×10^{-6}	40*

* Values obtained from literature [15-17].

Doubling the rate constant can reduce system pressure drop and exergy losses, ultimately reducing the SEC of hydrogen liquefaction. To evaluate the magnitude of the SEC reduction, the impact of an improved rate constant was estimated for 100 metric tonne per day hydrogen liquefaction plant that includes three OPC stages. While doubling the rate constant had negligible effect, a 100 times enhancement in k reduced exergy losses by 30% and cut the SEC by 0.11 kWh/kg LH_2. Such kinetic enhancements may be achievable with a higher Rh/Ru catalyst loading.

4. Conclusions

This study provides new insights into the performance of PGM catalysts for hydrogen OPC. Both Rh/Al_2O_3 and Ru/Al_2O_3 exhibited rate constants approximately twice that of the commercial IONEX catalyst, whereas Pt/Al_2O_3 showed negligible activity under the investigated conditions. Material characterisation indicated that PGM catalysed conversion is consistent with a dissociation–recombination mechanism, in contrast to the non-dissociative magnetic mechanism associated with IONEX. Further work will investigate the effects of activation gas type and

temperature on catalyst performance and examine hydrogen adsorption, binding, and dissociation on the catalyst surfaces under reaction conditions. Future studies will also evaluate catalytic activity at temperatures as low as 20 K, determine the influence of an externally applied magnetic field, and assess the effect of metal loading on catalyst performance. These investigations will provide a more comprehensive understanding of the factors governing PGM activity and support the development of more efficient catalysts for hydrogen liquefaction. Finally, this work will be followed by detailed process analysis and simulations of the impact of higher k values.

Acknowledgements

This work was supported by the Australian research council (ARC DECRA DE240100863), and the University of Sydney Nano Institute.

References

1. Fang, S., et al., *Dimensionless performance mapping of cryogenic plate-fin heat exchangers with ortho-para hydrogen continuous conversion for hydrogen liquefaction.* Energy, 2024. **313**: p. 133951.
2. Riaz, A., et al., *Significance of ortho-para hydrogen conversion in the performance of hydrogen liquefaction process.* International Journal of Hydrogen Energy, 2023. **48**(68): p. 26568-26582.
3. Jiao, F., et al., *Review of hydrogen ortho–para conversion: experimental data and reaction kinetics.* Reaction Chemistry & Engineering, 2024. **9**(11): p. 2846-2862.
4. Leachman, J.W., Ø. Wilhelmsen, and K.I. Matveev, *Cool Fuel: The Science and Engineering of Cryogenic Hydrogen*. 2025: Oxford University Press.
5. Mendoza-Moreno, P.V., G.J. Fulham, and E.J. Marek, *Harnessing the enigmatic ortho-para isomeric conversion for energy-efficient and low-carbon production of liquid hydrogen.* Cell Reports Sustainability, 2024. **1**(11).
6. Al Ghafri, S.Z., et al., *Hydrogen liquefaction: a review of the fundamental physics, engineering practice and future opportunities.* Energy & environmental science, 2022. **15**(7): p. 2690-2731.
7. Molecular Products Group. *IONEX Type OP Catalyst*. 31 July 2026]; Available from: https://www.molecularproducts.com/products/ionex-type-op-catalyst.
8. O'Neill, K.T., et al., *Hydrogen ortho-para conversion: process sensitivities and optimisation.* Chemical Engineering and Processing-Process Intensification, 2023. **184**: p. 109272.
9. Brooks, C.J., W. Wang, and D.P. Eyman, *Supported transition metal catalysts for para-to ortho-hydrogen conversion*. 1994.
10. Bahabadi, M.G., et al. *Improving the activity of ortho-para hydrogen conversion catalysts for hydrogen liquefaction*. in *CEC/ICMC 2025*. 2025. USA.
11. Eisenhut, S., C. Haberstroh, and C. Thomas, *Activation procedures for hydrous ferric oxide ortho-parahydrogen catalyst.* International Journal of Hydrogen Energy, 2026. **243**: p. 155685.
12. VICI Metronics. *P200 – Hydrogen Gas Purifier*. 31 July 2026]; Available from: https://www.vicimetronics.com/products/hydrogen-gas-purifier.
13. J-Science Lab Co., L. *Ortho–Para Hydrogen Analyzer DS-502*. IPROS 2022 21 November 2022 31 July 2026]; Available from: https://www.ipros.com/en/product/detail/2000576619/.
14. Wigner, E., *Uber die paramagnetische umwandlung von para-orthowasserstoff. III.* Z. Phys. Chem. B, 1933. **23**: p. 28-32.
15. Feulner, P. and D. Menzel, *The adsorption of hydrogen on ruthenium (001): Adsorption states, dipole moments and kinetics of adsorption and desorption.* Surface Science, 1985. **154**(2-3): p. 465-488.
16. Yates Jr, J., P. Thiel, and W. Weinberg, *The chemisorption of hydrogen on Rh (111).* Surface Science, 1979. **84**(2): p. 427-439.
17. Christmann, K., G. Ertl, and T. Pignet, *Adsorption of hydrogen on a Pt (111) surface.* Surface Science, 1976. **54**(2): p. 365-392.